NASA Technical Paper 1879

Meteoroid Bumper Experiment on Explorer 46

Donald H. Humes
Langley Research Center
Hampton, Virginia

NASA
National Aeronautics and Space Administration
Scientific and Technical Information Branch
1981

The NASA STI Program ... in Profile

Since its founding, NASA has been dedicated to ensuring U.S. leadership in aeronautics and space science. The NASA Scientific and Technical Information (STI) Program plays an important part in helping NASA maintain its leadership role.

The NASA STI Program provides access to the NASA STI Database, the largest collection of aeronautical and space science STI in the world. The Program is also NASA's institutional mechanism for disseminating the results of its research and development activities.

A number of specialized services help round out the Program's diverse offerings, including creating custom thesauri, translating material to or from 34 foreign languages, building customized databases, organizing and publishing research results.

For more information about the NASA STI Program, you can:

- **Phone** the NASA Access Help Desk at (301) 621-0390
- **Fax** your question to NASA Access Help Desk at (301) 621-0134
- Send us your question via the **Internet** to help@sti.nasa.gov
- **Write to:**

  NASA Access Help Desk
  NASA Center for AeroSpace Information
  800 Elkridge Landing Road
  Linthicum Heights, MD 21090-2934

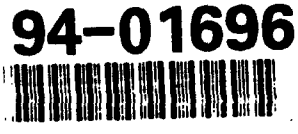

NASA CENTER FOR AEROSPACE INFORMATION

800 ELKRIDGE LANDING ROAD LINTHICUM HEIGHTS, MD 21090 (301) 621-0390

ATTN: (PHONE)
DATE OF REQUEST: 01/07/94
USER ID: 02672
ORDER CONTROL NUMBER: 940107095746
USER SECURITY LEVEL: SECRET RESTRICTED

ENCLOSED IS YOUR ORDER FOR 0001 HARDCOPY COPY **OF NASA ACCESSION NUMBER** N81-29155
TITLE: Meteoroid bumper experiment on Explorer 46
REPORT NUMBER: NASA-TP-1879

DOCUMENT CLASSIFICATION: UNCLASSIFIED
DISTRIBUTION LIMITATION STATEMENT: UNLIMITED

QUESTIONS CONCERNING THIS ORDER SHOULD BE DIRECTED TO DOCUMENT REQUEST SERVICES, NASA CASI (301) 621-0390
PLEASE INCLUDE YOUR ORDER CONTROL NUMBER WITH YOUR INQUIRY

02672-940107095746
DEPT OF DEFENSE
DEFENSE TECHNICAL INFORMATION CENTER
ATTN: DTIC-OCP/JOYCE CHIRAS
CAMERON STATION BLDG 5
ALEXANDRIA VA 22304

02672-940107095746
DEPT OF DEFENSE
DEFENSE TECHNICAL INFORMATION CENTER
ATTN: DTIC-OCP/JOYCE CHIRAS
CAMERON STATION BLDG 5
ALEXANDRIA VA 22304

SUMMARY

An experiment on the Explorer 46 spacecraft has provided the first accurate measurements of the effectiveness of a meteoroid bumper in reducing meteoroid penetrations. The bumper reduced the penetration flux by a factor of 30 and demonstrated a weight savings of a factor of 6.9 in the material needed to resist meteoroid penetration. The method of calculating the penetration flux recommended in the NASA space vehicle design criteria for meteoroid damage assessment was found to be very conservative, and changes have been suggested. The optimum distribution of material between a bumper and the main wall is discussed.

INTRODUCTION

Whipple (ref. 1) suggested that the damage to a spacecraft from meteoroid impacts could be greatly reduced by placing a thin shield around the spacecraft at some distance from the hull. Whipple envisioned that the shield, which he labeled a meteor bumper, would vaporize meteoroids upon impact, thus dissipating their penetrating powers.

The validity of the bumper concept was demonstrated in a number of laboratory studies (refs. 2 to 8). Even at impact speeds too low to cause vaporization, a bumper was seen to fragment the projectile and disperse the fragments over a large area of the main wall, giving the double-wall structure a much greater resistance to penetration than a single wall of the same thickness. However, all the laboratory tests were conducted at impact speeds less than the average meteoroid impact speed, and it is unclear how the data should be extrapolated to meteoroid velocities. No patterns were recognized in the data that could be used to formulate a general empirical penetration equation for double-wall structures.

Theoretical analyses have not considered the very complex fragmentation process and have addressed only the problem of the main-wall thickness required to withstand the blast load induced by a meteoroid that has been completely vaporized by the bumper (refs. 7 and 9, for example). These theories, which require an experimental determination of some quantities to give quantitative results, suggest that the meteoroid mass required to produce a blast-loading failure of the main wall varies with impact velocity as $V^{-0.75}$ to V^{-1}. But, the situation analyzed in these theoretical studies (i.e., a completely vaporized projectile) probably is not applicable to meteoroid impacts. Solid particles, which may be more lethal than the vapor cloud, will probably be produced even at meteoroid impact speeds when meteoroids are irregular in shape and nonhomogeneous in composition (ref. 10).

The lack of understanding of the behavior of double-wall structures during hypervelocity impact is reflected in the NASA space vehicle design criteria for meteoroid damage assessment (ref. 10). The recommendation in that document is that the resistance to meteoroid penetration of a double-wall structure be

estimated by performing hypervelocity impact tests at the highest speed tainable in the laboratory, and then extrapolating the results to meteoroid impact speeds by assuming that meteoroids of equal kinetic energy produce the same damage. This is clearly a conservative approach if the form of the theoretical results is correct (i.e., suggesting more meteoroid protection is required).

Even though the effectiveness of double-wall structures against meteoroids had not been demonstrated in space, the promise of great weight savings seen in the extrapolation of laboratory data led designers to use bumpers on a number of spacecraft. The bumper used on Skylab was counted on heavily to reduce the probability of a meteoroid penetration from approximately 0.05, which is unacceptable for a manned mission, to about 0.0001. Skylab survived; its hull was not penetrated during the manned mission or during the post-mission period. This flight experience, however, does not provide data on the effectiveness of that bumper. It does not even demonstrate that double-wall structures have a greater resistance to meteoroid penetration than a single wall because no penetrations were expected to occur, even without the bumper.

The survival of the pressurized photographic canisters on four of the five Lunar Orbiter spacecraft demonstrated that meteoroid bumpers are effective in reducing meteoroid penetration damage (ref. 11). The thermal blanket on that spacecraft acted as a bumper which protected the pressurized photographic canister. However, the small statistical sample (only five canisters were flown and only one canister was penetrated) resulted in only a poor definition of the effectiveness of the double wall, indicating that the double wall had the same penetration resistance as a single wall 10 to 840 percent thicker than the combined thickness of the two walls.

The first accurate measurement of the effectiveness of a bumper in reducing meteoroid penetrations was made on Explorer 46. Explorer 46 was an Earth-orbiting satellite dedicated to the study of meteoroids and meteoroid protection. Three meteoroid experiments were carried onboard the spacecraft. The meteoroid bumper experiment was the primary experiment. The secondary experiments were intended to measure the population of very small ($\approx 10^{-18}$ kg) meteoroids and the velocity of meteoroids. A malfunction onboard the spacecraft seriously degraded the secondary experiments. The measurements of the population of small meteoroids were limited to a few days after launch and a few days just prior to the termination of the experiment. The velocity measurements were lost altogether. The bumper experiment was only slightly affected by the malfunction.

This report contains a discussion of the results obtained with the Explorer 46 meteoroid bumper experiment and a comparison of those results with the results predicted using the method recommended in the NASA space vehicle design criteria for meteoroid damage assessment. A discussion of the failure modes for double-wall structures is included to illustrate the extent to which the Explorer 46 data apply to double-wall structures in general. The optimum distribution of material between the bumper and main wall is discussed to support the contention that the Explorer 46 double wall was not optimized and that, therefore, even more efficient double-wall structures can be constructed.

Identification of commercial products in this report is used to adequately describe the model. The identification of these commercial products does not constitute official endorsement, expressed or implied, of such products or manufacturers by the National Aeronautics and Space Administration.

SYMBOLS

A	area of experiment, m^2
A_{eff}	effective area of cell, m^2
E	kinetic energy of meteoroid that can just penetrate double-wall structure, J
$f_1(\gamma,x,y)$	fraction of view angle γ from point x,y on side 1 of detector panel that is unobstructed by other spacecraft components, dimensionless
$f_2(\gamma,x,y)$	fraction of view angle γ from point x,y on side 2 of detector panel that is unobstructed by other spacecraft components, dimensionless
G	defocusing factor to account for gravitational focusing of meteoroids near Earth, dimensionless
$g(V)$	meteoroid impact-velocity probability density function, $(m/s)^{-1}$
H	altitude of spacecraft above surface of Earth, Earth radii
K_1	material constant in single-wall penetration equation, $m^{0.625}s^{0.875}/kg^{0.519}$
K_2	constant in double-wall penetration equation, kg s^{α}/m^{α}
ℓ	length of detector panel, m
m	mass of meteoroid, kg
N_p	number of pressurized cell detectors penetrated
R	range of spacecraft from center of Earth, Earth radii
t	thickness of single wall, m
t_b	thickness of bumper, m
t_{mw}	thickness of main wall, m
V	impact velocity, m/s
w	width of detector panel, m

x	width coordinate of point on detector panel, m
y	length coordinate of point on detector panel, m
α	exponent of impact velocity in double-wall penetration equation, dimensionless
γ	view angle of space measured from normal to point on detector surface, rad
ζ	shielding factor to account for shielding of spacecraft by Earth, dimensionless
θ	Earth shielding angle, rad
ρ	density, kg/m^3
ρ_b	density of bumper material, kg/m^3
ρ_m	density of meteoroid, kg/m^3
τ	time, s
Φ	penetration flux, penetrations/m^2s
ϕ	cumulative meteoroid flux, impacts/m^2s

DESCRIPTION OF EXPERIMENT

The orbiting configuration of the Explorer 46 spacecraft is shown in figure 1. Basically, the spacecraft consisted of a central hub section, which housed the secondary experiments and telemetry system, and four deployable wings which were the target panels for the bumper experiment. Each wing consisted of three flat panels in a configuration that looked like a cross when viewed from the end. Each panel contained eight pressurized cells formed by joining two 50-μm-thick sheets of 21-6-9 stainless steel[1] by resistance welding. The pressurized cells were long, narrow cells running the length of the panel. In addition, there was a 25-μm-thick bumper of 21-6-9 stainless steel on each side of the panel. Figure 2 is a sketch of the panel construction. The 50-μm wall represented the hull or main wall of the double-wall structure being tested, while the 25-μm sheet was the bumper that essentially surrounded the main wall. The spacing between the walls was 13 mm. In addition to the welds that ran the length of the panels to isolate the cells from each other, there were five welds running the length of each cell to keep the cells flat and to provide a nearly constant spacing between the walls. A manifold at the end of each cell allowed the gas to occupy and flow freely through the entire cell volume.

[1] 21-6-9, now known as Nitronic 40: Registered trademark of Armco Steel Corp.

During launch, the panels were rolled up like window shades and the cells were not inflated. After the spacecraft was injected into Earth orbit, booms were used to unroll the wings, then the cells were pressurized. The booms provided the tension needed in the bumpers to maintain the 13-mm spacing between the bumper and the main wall.

It was intended that all four wings would extend to a length of 3.20 m, but a malfunction in the deployment apparatus left two opposing wings only partially deployed. It has been estimated, from the time the boom drive motor operated, that the partially deployed wings were extended to a length of 1.6 m. This malfunction created an unfavorable spacecraft inertia ratio and caused a transfer from the preferred spin stabilization mode (i.e., spinning about the axis of the rocket motor) to a rotational motion which invalidated the passive thermal design concept. As a result, the prime telemetry system and its battery power supply were left in constant sunlight. The consequent overheating resulted in a command anomaly and a decision to discontinue interrogation of the prime telemetry system. The data for the small-meteoroid population experiment were transmitted only through the prime telemetry system and were lost when that system was not interrogated. The unfavorable orientation of the spacecraft also left the meteoroid velocity detectors in sunlight which caused the front stations to develop a permanent electrical short. The data from the meteoroid bumper experiment were transmitted through a backup telemetry system which operated continuously when the spacecraft was in sunlight, so that no data were lost because of the malfunction.

The essential data obtained from the bumper experiment were the times at which each cell was penetrated by a meteoroid. Those penetrations were detected by observing the loss in pressure that accompanied the penetration. The cells were initially pressurized to 9.6×10^4 Pa with helium. Each cell contained a switch that was set to indicate whether the internal pressure was above or below 4.8×10^4 Pa. The switches were identified in the telemetry data so that the status of each particular cell could be monitored. The numbering system used to identify the 96 cells is shown in figure 1.

Explorer 46 was boosted into orbit on August 13, 1972, from the NASA Wallops Flight Center by a Scout D launch vehicle. The spacecraft achieved an orbit of 490 km by 815 km with an inclination of 38°. The attitude of the spacecraft was not known. The final interrogation of the experiment was made on January 29, 1975.

RESULTS

The data consisted of a readout of the state of each of the 96 pressurized cells (i.e., whether they were pressurized or unpressurized) obtained at various times during the experiment. A cell was considered to be unpressurized when the switch for that cell indicated that the internal pressure was below 4.8×10^4 Pa.

When the first interrogation of the spacecraft was made (30 min after the wing panels were deployed and the cells pressurized), it was observed that 95 cells were still pressurized while 1 cell (no. 81) was not.

During the next 829 days (the duration of the experiment), 52 more cells lost their pressure. At the conclusion of the experiment, 43 cells were still pressurized, while 53 cells were unpressurized.

The time at which each cell lost its pressure is given in table I. The time is generally known with an accuracy of about 1 day. For cell numbers 47 and 73, however, the uncertainty is about 7 days. During an 85-hr period between interrogations (which extended from day 266 to day 269 in 1972), three cells were penetrated. It is not known whether the pressure loss in these cells (nos. 49, 84, and 89) occurred simultaneously or at different times. Such a situation also existed during a 30-hr period between days 104 and 105 in 1973. During that period, two cells were penetrated (nos. 20 and 58).

There was one anomaly in the data. During the period from day 284 to day 343 in 1974, cell number 27 oscillated between the pressurized state and the unpressurized state. After day 343 in 1974, the cell remained in the unpressurized state. Times at which the cell changed states are given in table II. The table probably is not a complete list of all the changes that occurred between the pressurized and unpressurized states during that period because the spacecraft was usually interrogated only once or twice a day for about 2 min.

DISCUSSION OF RESULTS

Number of Meteoroid Penetrations

The cell that was unpressurized when the experiment was first interrogated (no. 81) was an end cell on one of the partially deployed wings, and may have become fouled during the faulty deployment process. The loss of pressure from this cell may have been caused by the malfunction instead of by a meteoroid penetration. Therefore, this cell was ignored when the data were analyzed.

The cell that oscillated between the pressurized state and the unpressurized state for 59 days (no. 27) may have suffered a near-threshold penetration which caused it to leak down very slowly. When the internal pressure approached the threshold of the sensor switch, thermal variations, which would result in pressure variations, could have caused the pressure to oscillate above and below the switch threshold. In this situation, the meteoroid penetration would have occurred at some undetermined time, long before the first indication that the cell was unpressurized. Because of this uncertainty, cell number 27 was also ignored when the data were analyzed.

Thus, analysis of the effectiveness of the bumper was based on data from 94 cells, 51 of which were penetrated by meteoroids during the experiment, 43 of which were not. It was assumed that the 51 penetrations were caused by 51 different meteoroids, although there is a possibility that two of the cells (nos. 84 and 89) were penetrated as the result of a single meteoroid impact. These two cells are very close together and may have been penetrated at essentially the same time. A large meteoroid could have passed directly through the two cells, or fragments thrown from the impact site on one cell could have gone through the other cell. If 50 meteoroids were actually responsible for the penetrations instead of the 51 meteoroids assumed, the mean value of the

penetration flux calculated would be in error by about 2 percent. Whether 50 or 51 meteoroid penetrations occurred is not very important because that introduces only a small error compared to the statistical error of ±24 percent inherent in calculating the penetration flux from 51 penetrations with 90-percent confidence.

The meteoroid penetrations actually occurred sometime before the switches indicated that a penetration had taken place, the difference being the time needed for the cells to leak down from a pressure of 9.6×10^4 Pa to 4.8×10^4 Pa. It was assumed that the leakdown times for the cells were small (compared to the 1-day uncertainty in the time at which the cells lost their pressure) and, therefore, did not have a significant effect on the interpretation of the data. For comparison, most of the pressurized cell detectors on Pioneers 10 and 11, which had about 1/50th the volume of the Explorer 46 cells, were calculated to have leakdown times less than 1 min (ref. 12).

Penetration Flux

The penetration flux is equal to N_p/AT where N_p is the number of meteoroid penetrations that occur in an area A of a structure during time T. It is a measure of the vulnerability of that structure to meteoroid penetration.

Two factors must be considered in establishing the area of the Explorer 46 experiment. First, the sensitive area of the experiment was not constant but decreased each time a cell was penetrated. Second, the view of space from the cells was partially obstructed by other panels so that the effective area of each cell was less than its actual area. For meteoroids approaching the spacecraft with equal probability from all directions, the effective area of a cell is

$$A_{eff} = \int_{x=0}^{w} \int_{y=0}^{\ell} \int_{\gamma=0}^{\pi/2} f_1(\gamma,x,y) \cos\gamma \, d\gamma \, dy \, dx + \int_{x=0}^{w} \int_{y=0}^{\ell} \int_{\gamma=0}^{\pi/2} f_2(\gamma,x,y) \cos\gamma \, d\gamma \, dy \, dx \quad (1)$$

where γ is the view angle of space measured from the normal to the detector surface, $f_1(\gamma,x,y)$ is the fraction of the view angle γ (from a point x,y on the detector panel) that is unobstructed by other spacecraft components on one side of the detector panel, $f_2(\gamma,x,y)$ is the corresponding function for the other side of the panel, w is the width of the detector panel, and ℓ is the length of the panel. The $\cos\gamma$ appears in equation (1) because the projected area of a surface element depends on the viewing angle. The effective area of each cell is given in table I. The actual area of each cell on the fully deployed panels was 0.322 m^2, while each cell on the partially deployed panels had an area of approximately 0.161 m^2. The effective area was 76 to 92 percent of the actual area depending on the cell location. Integrating the effective area of the unpenetrated cells as a function of time over the duration

of the experiment gives a total area-time product AT for the Explorer 46 bumper experiment of 9.92×10^8 m^2s.

The penetration flux measured for the double-wall structure on Explorer 46 was, therefore,

$$\Phi = \frac{51 \text{ penetrations}}{9.92 \times 10^8 \text{ } m^2s} = 5.14 \times 10^{-8} \frac{\text{penetration}}{m^2s} \quad (2)$$

Some uncertainty must be associated with this value because it was based on only 51 meteoroid penetrations. By use of the chi-square distribution to assess the uncertainty (in the manner suggested by Alvarez in ref. 13), the actual mean penetration flux for the double-wall structure was determined, with 90-percent confidence, to be between 4.0×10^{-8} and 6.5×10^{-8} penetration/m^2s.

The time history of the penetrations is shown in figure 3. The curve shows the time history that would be expected for a penetration flux of 5.14×10^{-8} penetration/m^2s if all the cells had an area equal to the average effective cell area, 0.204 m^2.

Effectiveness of Bumper

The effectiveness of a bumper or the effectiveness of a double-wall structure in reducing meteoroid penetrations is evaluated by comparing the penetration flux for the double wall with the penetration flux for a single wall of the same total thickness and same material, exposed to the same meteoroid environment.

The penetration flux for a single wall of stainless steel in near-Earth orbit is shown in figure 4 as a function of wall thickness. The single-wall curve in figure 4, developed by Alvarez (ref. 14), is based on: the Explorer 23 experiments (ref. 14), in which single walls of stainless steel (25 μm and 50 μm thick) were exposed to the near-Earth meteoroid environment; the meteoroid-penetration experiments conducted on the Pegasus satellite (penetration into aluminum sheets); and the meteor data obtained with ground-based radar and photographic systems. Consideration of the Pegasus and meteor data is responsible for the changing slope of the curve.

The penetration flux for the double-wall structure tested on Explorer 46 is shown at a thickness of 75 μm, which is the combined thickness of the bumper and the main wall. The penetration flux for the double-wall structure was much less (a factor of 30) than the penetration flux for a single wall of the same thickness, which demonstrates that a meteoroid bumper is indeed a very effective means of reducing meteoroid penetrations.

Efficiency Factor

Another way of evaluating the effectiveness of a double-wall structure is by determining the weight savings it provides over a single wall. The double-

wall structure was penetrated at the same rate as a 514-μm-thick single wall of the same material. Thus, the protection provided by a 514-μm-thick single wall can also be obtained with a 75-μm-thick double wall, a weight savings of a factor of 6.9. The efficiency factor, which is the ratio of the equivalent single-wall thickness to the actual thickness is, therefore, 6.9.

Distributions of Meteoroid Penetrations

For long periods of time during the experiment, meteoroid penetrations occurred almost exclusively in either the fully deployed wings or the partially deployed wings. This tendency is clearly illustrated in figure 5. At first it seemed that this would uncover a directionality factor in the meteoroid environment. However, attempts to discover the orbital distribution of the meteoroids that would have produced the observed results have been unsuccessful. The analysis is complicated by the fact that the attitude and rotational motion of the spacecraft were not known.

DESIGN APPLICATIONS

The efficiency factor of 6.9 for the double-wall structure on Explorer 46 cannot be applied to all double-wall structures. The efficiency factor may vary significantly with the distribution of material between the bumper and main wall, the spacing between the walls, and the material of which the walls are made.

The real contribution of the Explorer 46 data set is that it provides a test point for models used to calculate meteoroid penetration flux. A good model can be applied to future spacecraft wall designs of various configurations. This section shows how one model, that contained the NASA design criteria for meteoroid damage assessment, compares with the Explorer 46 data and discusses improvements that can be made in that model.

It is important to understand that the Explorer 46 experiment was not intended to establish the highest efficiency that a double-wall structure can have in reducing the weight of meteoroid protection. The distribution of material between the bumper and the main wall was not intentionally optimized. Efficiency factors greater than 6.9 probably can be attained. The discussion of optimum double-wall structures contained in this section is included to support the contention that the Explorer 46 double-wall structure was not optimum and that efficiency factors greater than 6.9 can be expected.

NASA Design Criteria for Meteoroid Damage Assessment

Spacecraft designers need a method of calculating the penetration flux for any double-wall structure, preferably a method that is based on a fundamental understanding of the meteoroid environment and hypervelocity impact phenomena. The method recommended in the NASA space vehicle design criteria for meteoroid damage assessment (ref. 10) only satisfies that requirement in part. It is

based on a fundamental understanding of the meteoroid environment, but admits to a lack of understanding of hypervelocity impact phenomena in double-wall structures.

The NASA design criteria use the basic model of the near-Earth meteoroid environment found in reference 15, which defines the size distribution, velocity distribution, mass density, and abundance of meteoroids. The model states that the average annual cumulative total flux ϕ, in impacts/m^2s, of meteoroids of mass m and greater, in kg, on a spacecraft is

$$\phi = G\,\zeta\,10^{\left[-19.658-1.962\,\log_{10}m-0.063(\log_{10}m)^2\right]}$$

for m between 10^{-15} kg and 10^{-9} kg, and

$$\phi = G\,\zeta\,10^{(-18.009-1.213\,\log_{10}m)}$$

for m greater than 10^{-9} kg. The factor G accounts for gravitational focusing of meteoroids near the Earth and is equal to

$$G = \frac{0.43}{R} + 0.57$$

where R is the range of the spacecraft from the center of the Earth, in Earth radii. The factor ζ accounts for the shielding provided by the Earth and

$$\zeta = \frac{1 + \cos\vartheta}{2}$$

with

$$\vartheta = \sin^{-1}\left(\frac{R}{R + H}\right)$$

where H is the altitude of the spacecraft above the surface of the Earth, in Earth radii. The model uses the meteoroid velocity distribution reproduced in figure 6, which has a mean of 20 km/s. The assumed density for meteoroids is 500 kg/m^3.

The NASA design criteria do not provide a model for the penetration of double-wall structures. Instead, they recommend that the penetration resistance of a double-wall structure to meteoroid impacts be established by testing the structure in a hypervelocity impact laboratory at the highest speeds attainable and extrapolating the results to meteoroid impact velocities by assuming that meteoroids of equal kinetic energy have equal penetrating capabilities. It is recommended that glass (ρ = 2300 kg/m^3) or syntactic foam (ρ = 900 kg/m^3) be used as projectiles to simulate low-density cometary meteoroids.

Hypervelocity impact tests were conducted to evaluate the penetration resistance of the Explorer 46 double-wall structure so that the penetration flux could be calculated using the NASA design criteria and the accuracy of this method could be checked. The wall thicknesses were scaled up a factor of 8 for some of the tests and a factor of 16 for the others, because it was difficult to use the tiny projectiles required to obtain near-threshold penetrations in the actual Explorer 46 material. Nylon projectiles were used because they were the lowest density projectiles available (ρ = 1100 kg/m^3) and, thus, would best simulate low-density cometary meteoroids. The objective of the tests was to determine the minimum particle mass that would cause the main wall to be punctured as a function of the particle velocity. The data from the hypervelocity impact tests are given in table III. The data were applied to the Explorer 46 double wall by linearly scaling the wall thicknesses and the projective diameter down to the size of the flight hardware. The results are shown in figure 7. Each data point shows the impact speed and the scaled particle mass for a single test. An open symbol indicates that both walls were penetrated, while a closed symbol means the main wall was not penetrated.

It was noticed that failure of the main wall always resulted from individual stainless-steel bumper fragments penetrating the main wall.

At impact speeds less than 4 km/s, the joint conditions of particle mass and impact speed which will cause a failure are clearly defined. Above 4 km/s, the threshold mass appears to be about 8.5×10^{-10} kg and a weak function of impact speed. Projectiles with a scaled mass of 8.5×10^{-10} kg would sometimes penetrate the structure, sometimes not, with no clear relationship to the impact speed. No penetrations occurred when projectiles with a scaled mass of 5.6×10^{-10} kg were used, even at the highest impact speed obtained, 6.9 km/s. It is unclear what form the penetration resistance curve would take at higher impact speeds. According to the recommendation in the NASA design criteria, it should be assumed that meteoroids with kinetic energy in excess of 0.0134 to 0.0203 J will penetrate the Explorer 46 double-wall structure, because at the highest impact speed tested (6.9 km/s), the mass required to penetrate the structure was between 5.6×10^{-10} kg and 8.5×10^{-10} kg.

When that criterion for the penetration resistance is used, along with the model of the near-Earth meteoroid environment, to calculate the penetration flux Φ for the Explorer 46 double-wall structure using equation (8) (see ref. 11),

$$\Phi = \int_{V=0}^{\infty} \int_{m=2EV^{-2}}^{\infty} \frac{\partial \phi}{\partial m} g(V)\, dm\, dV \tag{8}$$

the result is a penetration flux of 3.22×10^{-7} to 4.27×10^{-7} penetration/m^{2}s. If the intent of the kinetic-energy scaling in the design criteria was to provide a conservative estimate of the meteoroid hazard, it was successful. The quantity E in equation (8) is the kinetic energy that a meteoroid must have to cause a threshold penetration in the main wall.

Penetration of the double-wall structure on Explorer 46 apparently does not depend on the kinetic energy of the meteoroid, but on a parameter that has a weaker dependency on velocity. If it is assumed that the penetration resistance of double-wall structures is of the form $m = K_2 v^{\alpha}$, then α must be between 0.2 and 0.6 for the calculated penetration flux (using eq. (8)) to agree with the measured value of 5.14×10^{-8} penetration/m^2s. The exponent α must be 0.2 if the threshold mass for penetration is 8.5×10^{-10} kg at 6.9 km/s and must be 0.6 if the threshold mass for penetration is 5.6×10^{-10} kg at that velocity. (See fig. 8.) The positive exponent implies that, as the impact speed increases, the damage produced by a given size particle decreases. That is not unusual for a double-wall structure, nor difficult to understand. It has been observed in the laboratory (refs. 3 and 7) that the damage from projectile fragments decreases as the impact speed increases. The reason is that, at higher impact speeds, the projectile and the bumper are more thoroughly fragmented and the smaller fragments, despite their higher speeds, do not penetrate as deeply.

The Explorer 46 experiment shows that changes must be made in the methods recommended in the NASA design criteria for calculating the penetration flux for double-wall structures, if more accurate calculations are desired. Before suggesting specific changes, it is necessary to understand the different failure modes that can occur in double-wall structures.

Failure Modes for Double-Wall Structures

Two failure modes have been observed for double-wall structures during hypervelocity impact studies: (1) penetration of the main wall by individual fragments of bumper or projectile material; and (2) stress failures of the main wall caused by blast loading from a highly fragmented or vaporized projectile (with or without pits created by fragments contributing to the failure by acting as weak points where cracks are initiated). (See ref. 10.)

The stress on the main wall caused by blast loading can be reduced by increasing the spacing between the bumper and the main wall. That allows the fragmented or vaporized projectile cloud to disperse more extensively. Large spacings should be used on spacecraft whenever possible so that the probability of blast-loading failure becomes small, ideally insignificant, when compared to the penetration by fragments.

When the spacings used are large enough to essentially eliminate blast loading as a failure mode, penetration by individual fragments is the dominant failure mode. Increasing the spacing beyond that needed to eliminate blast loading does not provide increased penetration resistance, because the penetration capability of a fragment is not affected by the distance it travels.

The Explorer 46 double-wall structure had a very large spacing between the bumper and the main wall (173 times the total thickness of the bumper and main-wall material) so that blast-loading failures would be eliminated and the fragment penetration failure mode could be studied. Thus, the Explorer 46 experiment was designed to take full advantage of a bumper's best feature - its ability to disperse the meteoroid energy over a large area of the main wall.

The Explorer 46 data suggest that, when large spacings are used so that blast-loading failures are not a concern, the meteoroid mass required to penetrate a double-wall structure at meteoroid impact speeds should be assumed to be less than or equal to the projectile mass needed to penetrate the structure in laboratory tests performed at the highest possible impact speed. The laboratory tests would have to be performed at a speed great enough to fragment the projectile for the criteria to be valid. When large spacings are used, a double-wall structure is more nearly mass sensitive than kinetic-energy sensitive at meteoroid impact speeds.

When large spacings cannot be used and the possibility of blast-loading failures exist, a different criterion must be used. As the impact speed increases, the mass required to cause a blast-loading failure must decrease, because the main wall can only withstand an impulse of a certain magnitude. McMillan (ref. 7) concluded, as the result of theoretical studies, that the mass required to cause blast-loading failure will vary as V^{-1} (i.e., failure is related to the momentum of the meteoroid). But there have been no tests in space of double-wall structures (with small spacings) that would fail because of blast loading, so the theory has not been confirmed. Until such an experiment has been performed, conservative designers may wish to follow the recommendation in the NASA design criteria and assume that meteoroids of equal kinetic energy cause equal damage to double-wall structures with small spacings.

Just how far the bumper and main wall must be separated before the spacing can be considered large enough to essentially eliminate blast-loading failures is not known, but if the Explorer 46 spacing was large enough, as it appears it was, then a spacing equal to 173 times the thickness of the double-wall material would seem to be sufficient. Additional flight tests would be required to determine the extent to which the spacing could be reduced.

Optimum Double-Wall Structures

It may be possible to construct double-wall structures that provide a greater weight savings than that indicated by the efficiency factor of 6.9 measured by the Explorer 46 experiment. It is suspected that the double-wall structure tested did not make optimum use of the 75-μm thickness of stainless-steel material. The structure may have had a greater penetration resistance if some of the bumper material had been transferred to the main wall. Such a distribution of material would have been used in the experiment if manufacturing and fabrication problems could have been overcome.

The redistribution of bumper and main-wall material may have improved the penetration resistance of the structure, because the failure of the main wall, as observed in the laboratory tests, was caused by bumper fragments. If the bumper had been thinner and the main wall thicker, then smaller, less damaging bumper fragments would have been created and would have impinged on a more resistive main wall.

There are two components of the fragment field that can penetrate the main wall - bumper fragments and meteoroid fragments. In trying to optimize the distribution of material between the bumper and the main wall, consideration must

be given to both components. As the bumper is made thinner, the bumper fragments produced become smaller and less damaging, but the projectile fragments become larger and more damaging because lower stresses are produced throughout the projectile. On the other hand, thick bumpers more completely destroy the projectile, but produce larger bumper fragments in doing so.

If a bumper is thin enough, no bumper fragments will be created which are large enough to penetrate the main wall at the velocity imparted to them by the meteoroid. In this situation, the bumper-fragment field no longer poses a threat to the main wall, leaving the meteoroid fragments as the only hazard. The optimum distribution of material between the bumper and the main wall for protection against easily fragmented particles (like meteoroids are expected to be) may be that in which the bumper contains as much material as it can without producing fragments capable of penetrating the main wall.

In order to estimate this optimum distribution of material, it was assumed that the largest bumper fragments produced are compact particles whose size is equal to the thickness of the bumper. Further, it was assumed that the speed of the fragments is equal to the meteoroid impact speed. This assumption is conservative because the bumper-fragment speed will not exceed the meteoroid impact speed when the density of the meteoroid material is much less than that of the bumper material. The main-wall thickness that can be penetrated by the bumper fragments can be calculated using the single-wall penetration equation in reference 10. That equation is

$$t = K_1 m^{0.352} \rho_m^{1/6} V^{0.875} \tag{9}$$

where t is the thickness of a single wall, in m, that can be penetrated by a particle of mass m, in kg, density ρ, in kg/m^3, and velocity V, in m/s. A constant associated with the main-wall material K_1 is equal to 2.73×10^{-5} $m^{0.625} s^{0.875} / kg^{0.519}$ for stainless steel. The particle mass assumed for the bumper fragments is

$$m = \frac{\rho_b \pi t_b^3}{6} \tag{10}$$

where ρ_b is the density of the bumper material and t_b is the thickness of the bumper. Since the fragments strike the main wall at the meteoroid impact speed, the main-wall thickness that the fragments can penetrate t_{mw} is

$$t_{mw} = K_1 \left(\frac{\rho_b \pi t_b^3}{6} \right)^{0.352} \left(\rho_b^{1/6} V^{0.875} \right) \tag{11}$$

The bumper thickness that will produce fragments just capable of penetrating a main wall of a given thickness can be obtained by solving equation (11) for t_b.

$$t_b = \frac{t_{mw}^{0.947}}{(0.806)K_1^{0.947}\rho_b^{0.491}v^{0.829}} \qquad (12)$$

If the bumper thickness is kept less than that calculated with equation (12), then bumper fragments are not a threat to penetrate the main wall.

Solving equation (12) for the 50-μm-thick stainless-steel main wall used on Explorer 46 suggests that, for the average meteoroid impact speed of 20 km/s, a stainless-steel bumper that is 7.3 μm thick will produce fragments just capable of penetrating the main wall. Because the Explorer 46 bumper was much thicker (25 μm), it would produce fragments that would easily penetrate the main wall. The threat of bumper fragments penetrating the Explorer 46 main wall existed for all meteoroid impact speeds above 4.5 km/s, according to equation (12).

The optimum bumper for the 50-μm main wall varies from 13 μm for 10 km/s impacts to 5 μm for 30 km/s impacts. Thus, the optimum distribution of material between the bumper and the main wall occurs when 0.1 to 0.2 of the total material is in the bumper. There is a small scaling effect in the single-wall penetration equation (eq. (9)) which suggests that the fraction of the material used in the bumper should be decreased slightly as the total thickness of the double-wall structure increases.

CONCLUSIONS

The meteoroid bumper experiment on Explorer 46 showed that a bumper is an effective device for reducing meteoroid penetrations. The double-wall structure reduced the penetration flux by a factor of 30 from that expected for a single wall of the same thickness, and it provided the same protection as a 514-μm-thick single wall, which means it provided a weight savings of a factor of 6.9.

Hypervelocity impact tests in the laboratory implied that failure of the Explorer 46 double-wall structure occurred when bumper fragments penetrated the main wall. Blast-loading failures of the main wall did not occur because a very large spacing was used between the bumper and the main wall.

The method of calculating the penetration flux for a double-wall structure recommended in the NASA design criteria for meteoroid damage assessment, which calls for extrapolation of hypervelocity impact data to meteoroid impact speeds by assuming that meteoroids of equal kinetic energy produce equal damage to a double-wall structure, is not accurate. The calculated penetration flux for the Explorer 46 double-wall structure was conservative (high) by more than an order of magnitude. When large spacings are used so that blast-loading failures are not a threat, a more accurate estimate of the penetration flux can be obtained from the laboratory data by assuming that meteoroids of equal mass produce equal damage to a double-wall structure, regardless of their velocity.

Even greater effectiveness may have been achieved if the distribution of material between the bumper and the main wall in the Explorer 46 experiment could have been optimized by transferring some of the bumper material to the main wall. Engineering problems prevented the experiment from being optimized. The optimum distribution was calculated to be one in which the bumper contains about 0.1 to 0.2 of the available material.

Langley Research Center
National Aeronautics and Space Administration
Hampton, VA 23665
June 4, 1981

REFERENCES

1. Whipple, F. L.: Meteorites and Space Travel. Astron. J., vol. 52, no. 5, Feb. 1947, p. 131.

2. Nysmith, C. Robert; and Summers, James L.: An Experimental Investigation of the Impact Resistance of Double-Sheet Structures at Velocities to 24,000 Feet Per Second. NASA TN D-1431, 1962.

3. Humes, Donald H.: An Experimental Investigation of the Effectiveness of Single Aluminum Meteoroid Bumpers. NASA TN D-1784, 1963.

4. Humes, Donald H.: Influence of the Bumper and Main Wall Material on the Effectiveness of Single Meteoroid Bumpers. NASA TN D-3104, 1965.

5. Lundeberg, J. F.; Stern, P. H.; and Bristow, R. J.: Meteoroid Protection for Spacecraft Structures. NASA CR-54201, 1965.

6. Swift, H. F.; Carson, J. M.; and Hopkins, A. K.: Ballistic Limits of 6061-T6 Aluminum Bumper Systems. AFML-TR-67-324, U.S. Air Force, Oct. 1967.

7. McMillan, A. R.: Experimental Investigations of Simulated Meteoroid Damage to Various Spacecraft Structures. NASA CR-915, 1968.

8. Nysmith, C. Robert: An Experimental Impact Investigation of Aluminum Double-Sheet Structures. AIAA Paper No. 69-375, Apr.-May 1969.

9. Madden, Richard: Ballistic Limit of Double-Walled Meteoroid Bumper Systems. NASA TN D-3916, 1967.

10. Meteoroid Damage Assessment. NASA Space Vehicle Design Criteria (Structures). NASA SP-8042, 1970.

11. Humes, Donald H.: Calculation of the Penetration Flux for a Multiwall Structure on the Lunar Orbiter Spacecraft. NASA TN D-5455, 1969.

12. Humes, Donald H.: Calculation of the Leak-Down Times for Pressurized Cell Meteoroid Penetration Detectors. Description of the Meteoroid Detection Experiment Flown on the Pioneer 10 and 11 Jupiter Flyby Missions, Robert L. O-Neal, compiler, NASA TN D-7691, 1974, pp. 103-121.

13. Alvarez, J. M.: Statistical Analysis of Meteoroid Penetration Data Including Effects of Cutoff. NASA TN D-5668, 1970.

14. Alvarez, Jose M.: Preliminary Meteoroid-Penetration Model. The Explorer XXIII Micrometeoroid Satellite - Description and Results for the Period November 6, 1964, Through November 6, 1964, Robert L. O'Neal, compiler, NASA TN D-4284, 1968, pp. 85-89.

15. Meteoroid Environment Model - 1969 [Near Earth to Lunar Surface]. NASA Space Vehicle Design Criteria (Environment). NASA SP-8013, 1969.

TABLE I.- TIMES AT WHICH PRESSURIZED CELLS

WERE PENETRATED BY METEOROIDS

[Readings in year, day of year, hours, minutes, and seconds; start - 72 226 15 49 11; end - 75 029 18 15 39]

Cell no.	Effective area, m^2	Last pressurized y d h m s	First unpressurized y d h m s
1	0.296	73 167 17 11 57	73 168 21 07 17
2	.296	End	---
3	.295	End	---
4	.292	73 100 18 49 15	73 101 23 50 07
5	.289	73 105 11 02 51	73 106 16 06 36
6	.285	72 320 11 41 49	72 321 05 38 13
7	.280	72 255 22 07 24	72 257 02 36 45
8	.270	End	---
9	.249	72 240 08 35 25	72 241 10 43 37
10	.246	74 064 00 45 58	74 065 01 05 02
11	.250	End	---
12	.275	End	---
13	.275	End	---
14	.250	End	---
15	.246	End	---
16	.249	End	---
17	.269	74 308 13 29 50	74 309 16 02 22
18	.279	74 323 05 57 30	74 324 17 22 18
19	.285	74 083 03 57 02	74 084 17 41 05
20	.289	73 104 05 21 20	73 105 11 01 07
21	.291	End	---
22	.294	End	---
23	.295	End	---
24	.294	74 057 01 37 41	74 058 05 23 58
25	.136	End	---
26	.137	End	---
27	.136	(*)	(*)
28	.135	73 025 20 01 44	73 026 13 25 28
29	.134	73 317 02 40 50	73 318 12 57 26
30	.132	End	---
31	.129	72 290 20 56 15	72 291 08 26 26
32	.123	73 074 11 17 22	73 075 22 11 15
33	.120	72 257 02 38 29	72 257 22 59 31
34	.118	End	---
35	.119	End	---
36	.130	End	---
37	.130	End	---

*See table II.

TABLE I.- Continued

Cell no.	Effective area, m^2	Last pressurized y d h m s	First unpressurized y d h m s
38	0.119	End	---
39	.118	End	---
40	.120	End	---
41	.123	73 288 19 42 42	73 289 11 21 38
42	.128	End	---
43	.131	End	---
44	.133	End	---
45	.134	72 361 12 22 55	72 362 22 29 19
46	.136	72 311 01 18 33	72 312 15 06 04
47	.136	73 184 00 00 00	73 190 15 04 36
48	.135	72 250 06 17 28	72 251 06 43 47
49	.296	72 266 05 03 26	72 269 18 08 16
50	.296	End	---
51	.295	74 066 01 30 22	74 067 21 03 37
52	.292	72 249 04 14 04	72 250 06 15 39
53	.289	72 228 03 59 26	72 228 05 40 24
54	.285	End	---
55	.280	74 322 13 07 30	74 323 05 52 17
56	.270	End	---
57	.249	End	---
58	.246	73 104 05 21 20	73 105 11 01 07
59	.250	End	---
60	.275	73 141 20 26 02	73 142 13 41 52
61	.275	End	---
62	.250	End	---
63	.246	72 226 17 32 10	72 226 18 38 12
64	.249	74 179 22 08 00	74 180 22 27 51
65	.269	End	---
66	.279	End	---
67	.285	74 224 01 35 19	74 225 01 56 55
68	.289	74 036 17 20 17	74 038 17 29 09
69	.291	73 163 01 36 59	73 164 00 15 00
70	.294	End	---
71	.295	End	---
72	.294	74 108 03 31 56	74 109 07 19 51
73	.136	74 247 12 26 11	74 254 14 54 17
74	.137	72 265 04 39 35	72 266 05 01 41
75	.136	73 348 15 28 05	73 349 14 42 57
76	.135	73 057 00 33 25	73 058 19 32 38
77	.134	72 301 02 34 12	72 303 23 15 50
78	.132	73 327 20 36 05	73 328 09 24 42
79	.129	End	---
80	.123	75 007 07 09 40	75 008 09 11 18

TABLE I.- Concluded

Cell no.	Effective area, m^2	Last pressurized y d h m s	First unpressurized y d h m s
81	0.120	---	Start
82	.118	End	---
83	.119	End	---
84	.130	72 266 05 03 26	72 269 18 08 16
85	.130	End	---
86	.119	End	---
87	.118	End	---
88	.120	End	---
89	.123	72 266 05 03 26	72 269 18 08 16
90	.128	73 032 06 43 27	73 033 12 53 07
91	.131	74 288 08 43 11	74 289 11 00 36
92	.133	74 021 06 16 50	74 022 20 07 22
93	.134	72 281 11 34 29	72 282 13 43 01
94	.136	74 054 16 50 26	74 055 18 52 09
95	.136	72 360 02 25 20	72 361 12 21 06
96	.135	72 269 18 10 20	72 270 22 02 28

TABLE II.- TIMES AT WHICH CELL NUMBER 27 CHANGED

PRESSURE STATES

[Times given in year, day of year, hours, minutes, and seconds]

Change of state[a]	Time interval	
	y d h m s	y d h m s
P to U	74 284 10 40 18	74 285 04 05 17
U to P	74 285 04 07 15	74 286 09 35 22
P to U	74 288 08 43 11	74 289 11 00 36
U to P	74 289 11 01 48	74 289 11 01 52
P to U	74 289 11 02 26	74 289 11 58 47
U to P	74 290 07 34 00	74 290 07 34 05
P to U	74 290 07 36 26	74 291 12 38 48
U to P	74 300 17 36 31	74 301 19 36 21
P to U	74 306 16 14 16	74 308 13 26 22
U to P	74 328 02 25 50	74 328 02 25 55
P to U	74 329 04 30 37	74 330 01 22 31
U to P	74 330 01 23 04	74 330 01 23 09
P to U	74 330 01 25 49	74 331 01 42 36
U to P	74 331 01 43 26	74 331 01 43 32
P to U	74 331 01 44 43	74 332 02 02 22
U to P	74 332 02 04 02	74 332 02 04 03
P to U	74 332 02 05 48	74 333 02 22 12
U to P	74 343 08 25 05	74 343 08 25 10
P to U	74 343 08 26 21	74 343 08 42 18

[a]P - pressurized, U - unpressurized.

TABLE III.- HYPERVELOCITY IMPACT DATA ON SCALED-UP EXPLORER 46 DOUBLE-WALL STRUCTURES

Test no.	Bumper[a] thickness, mm	Main-wall[a] thickness, mm	Spacing, mm	Projectile[b]		Penetration of main wall
				Mass, mg	Velocity,[c] km/s	
1	0.20	0.40	50.8	3.5	3.3	Yes
2	↓	↓	↓	↓	2.8	Yes
3	↓	↓	↓	↓	2.3	No
4	↓	↓	12.7	↓	2.6	No
5	.40	.80	50.8	5.4	5.4	Yes
6	↓	↓	↓	↓	4.3	Yes
7	↓	↓	↓	↓	4.0	Yes
8	↓	↓	↓	↓	2.8	No
9	↓	↓	↓	↓	5.9	Yes
10	↓	↓	↓	↓	3.6	Yes
11	↓	↓	↓	↓	2.7	No
12	.40	.80	50.8	3.5	3.8	No
13	↓	↓	↓	↓	5.4	No
14	↓	↓	↓	↓	5.7	No
15	↓	↓	↓	↓	4.8	No
16	↓	↓	↓	↓	4.5	Yes
17	↓	↓	↓	↓	6.1	Yes
18	↓	↓	↓	↓	4.4	Yes
19	↓	↓	↓	↓	6.3	No
20	↓	↓	↓	↓	6.7	No
21	↓	↓	↓	↓	6.9	Yes
22	.40	.80	50.8	2.3	5.7	No
23	↓	↓	↓	↓	5.1	No
24	↓	↓	↓	↓	4.1	No
25	↓	↓	↓	↓	6.9	No
26	↓	↓	↓	↓	6.4	No

[a]Stainless steel.
[b]Nylon spheres.
[c]Normal to structure surface.

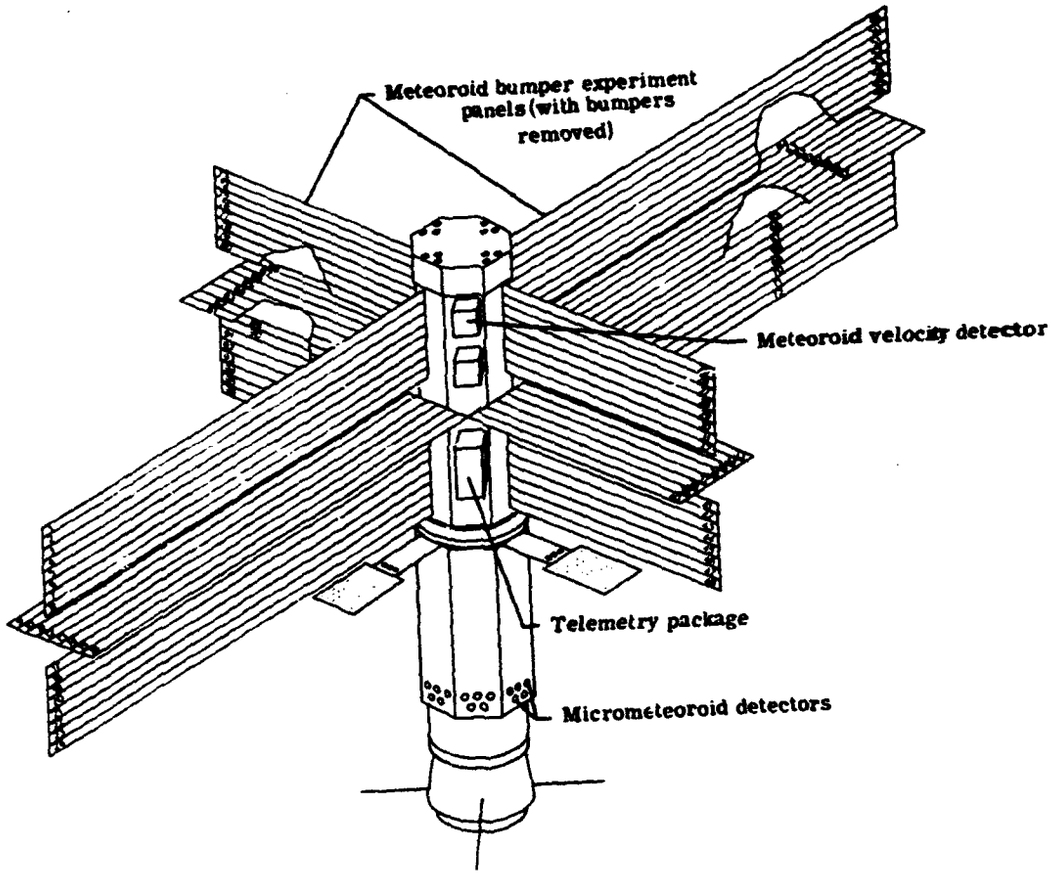

Figure 1.- Drawing of Explorer 46 spacecraft (with bumpers removed) showing numbering system used to identify pressurized cells for meteoroid bumper experiment.

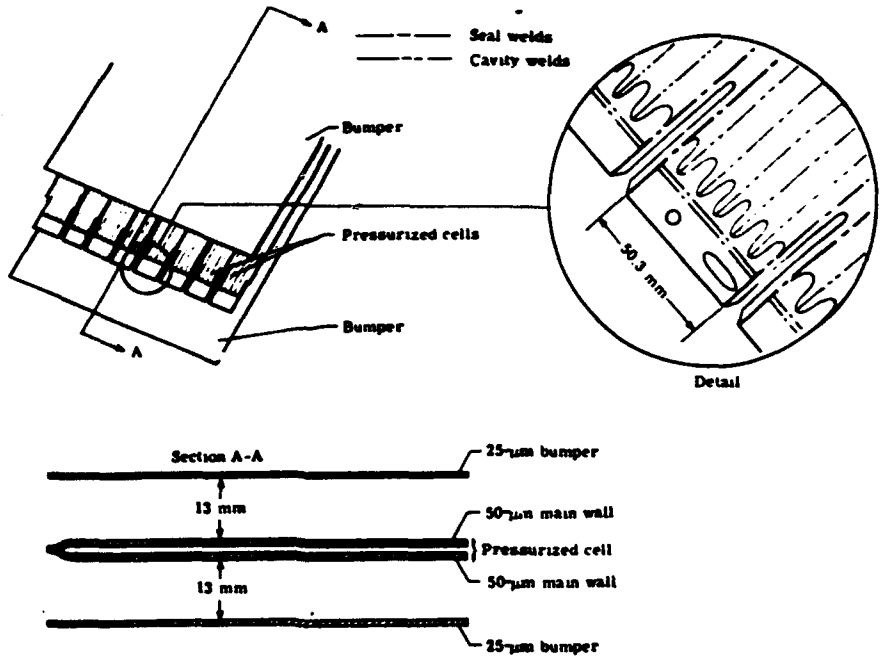

Figure 2.- Drawing of panel with bumpers showing double-wall structure tested on Explorer 46. All material was 21-6-9 stainless steel.

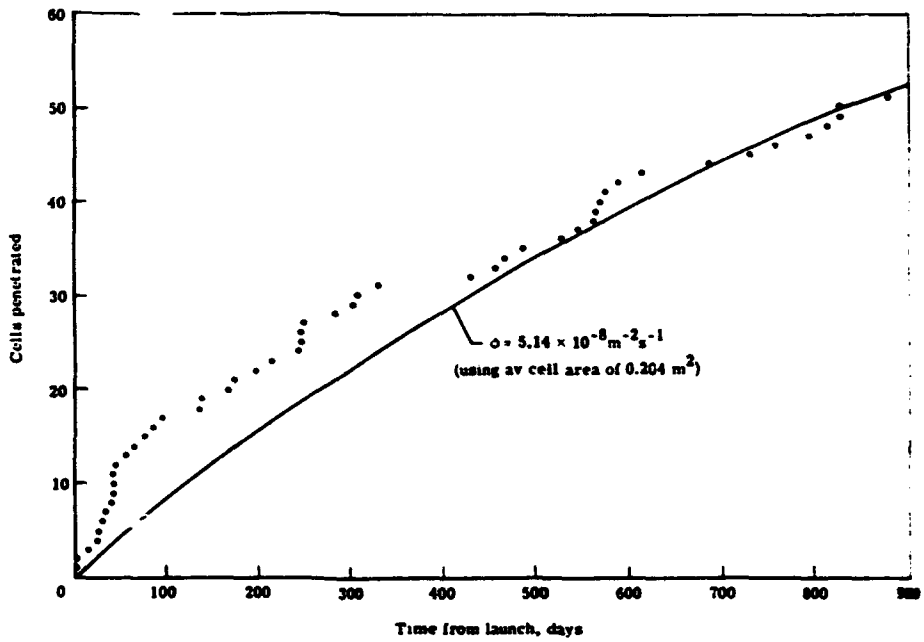

Figure 3.- Time history of penetration of cells on Explorer 46 meteoroid bumper experiment.

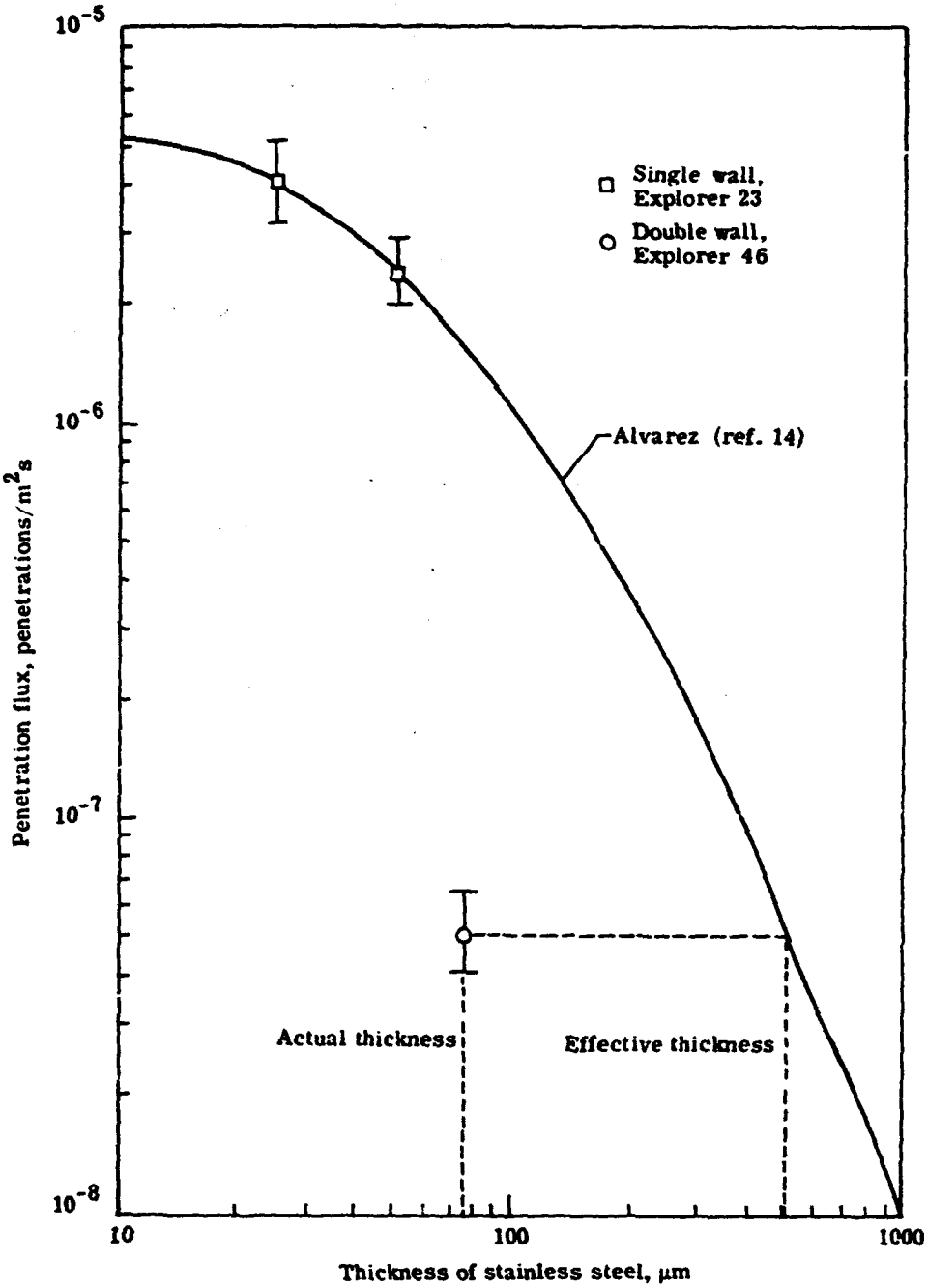

Figure 4.- Penetration flux for single stainless-steel walls and Explorer 46 double-wall stainless-steel structure, with 90-percent confidence limits.

THIS

PAGE

IS

MISSING

IN

ORIGINAL

DOCUMENT

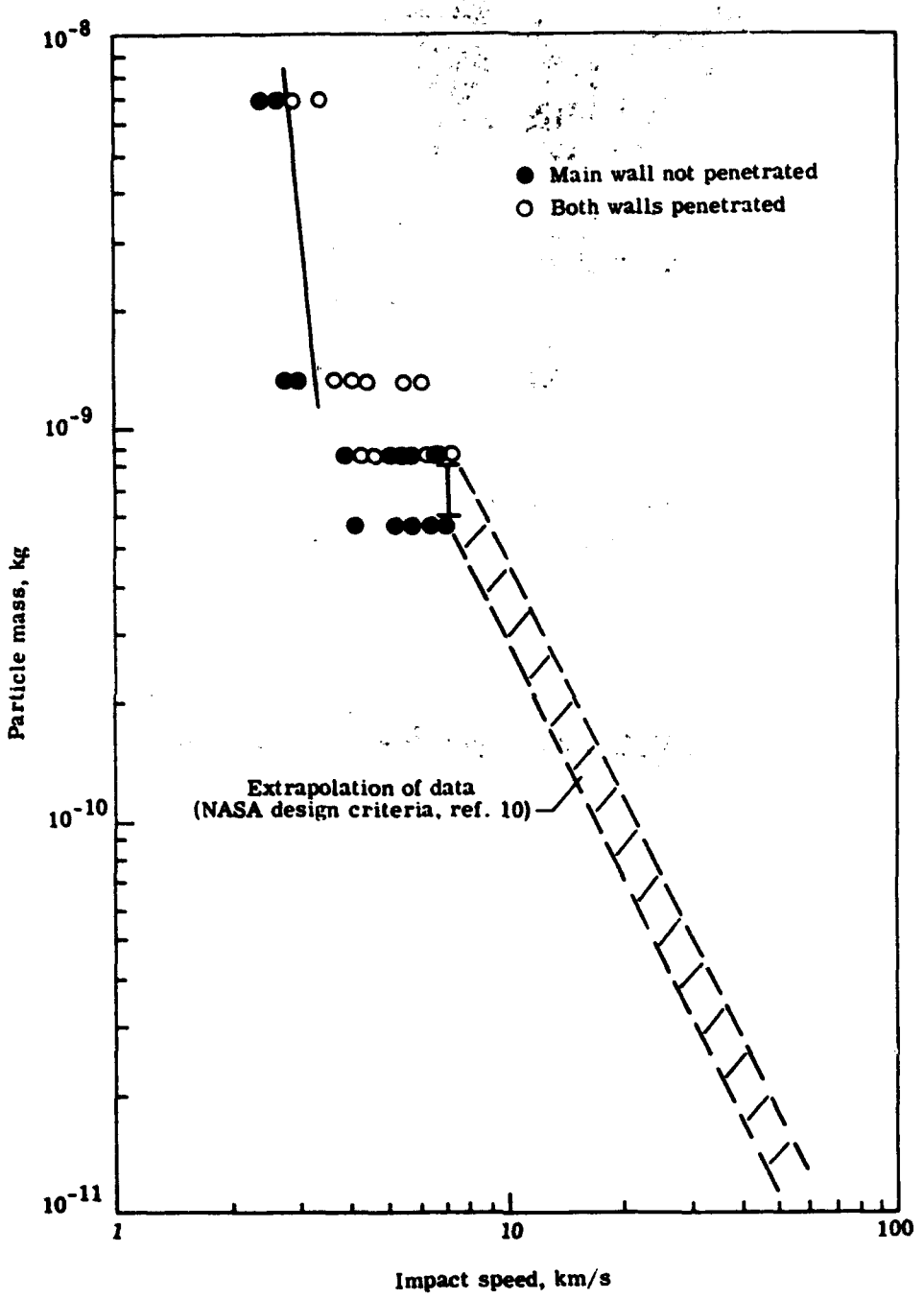

Figure 7.- Penetration resistance of Explorer 46 double-wall structure, scaled from hypervelocity impact data (table III).

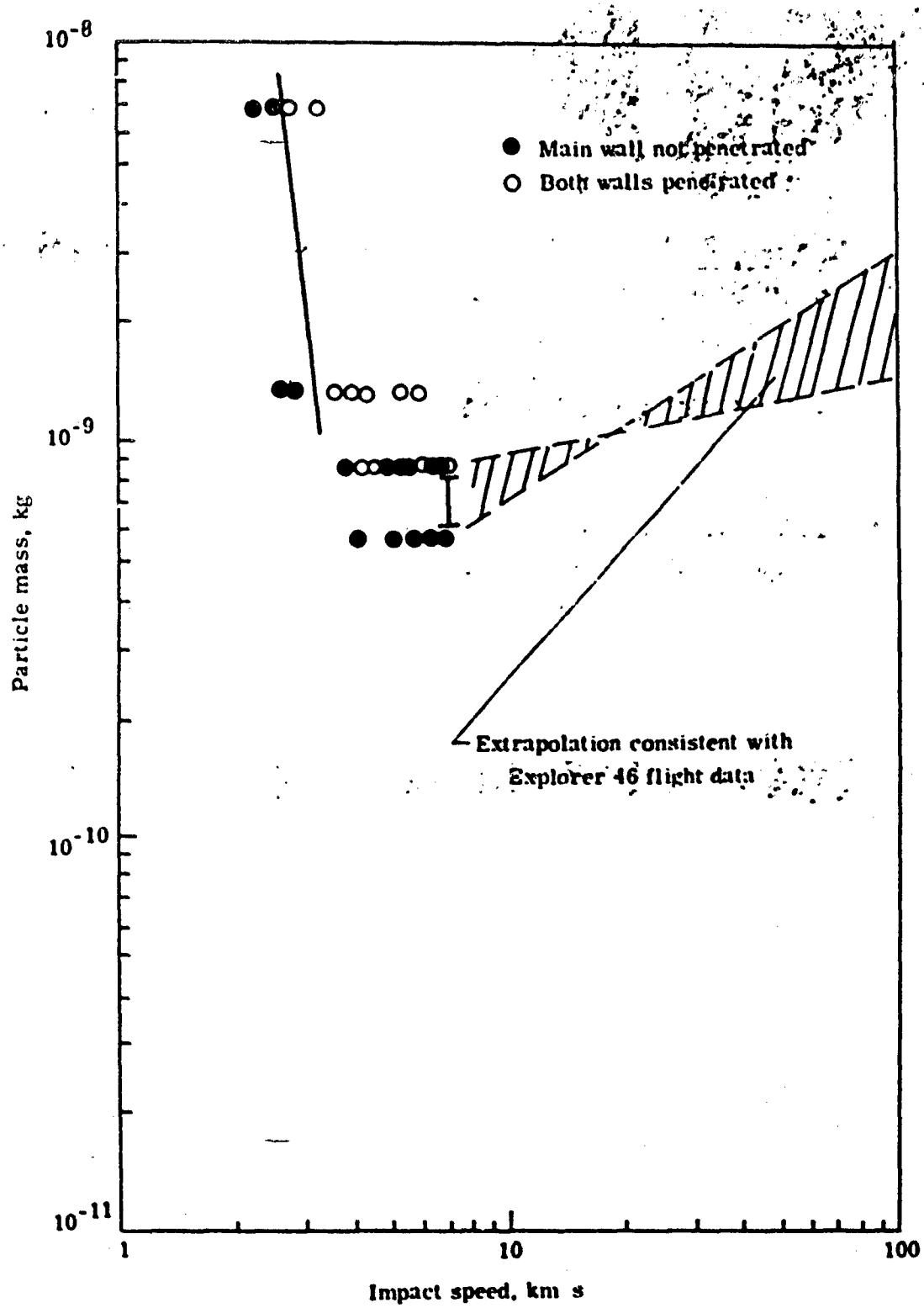

Figure 8.- Penetration resistance of Explorer 46 double-wall structure, showing extrapolations of data that are consistent with measured penetration flux of 5.14×10^{-8} penetration/m^2s.